*Chinese Journal of*
**POLYMER SCIENCE**

RESEARCH ARTICLE

https://doi.org/10.1007/s10118-023-2930-6
*Chinese J. Polym. Sci.* **2023**, *41*, 745–759

# Stride Strategy to Enable a Quasi-ergodic Search of Reaction Pathways Demonstrated by Ring-opening Polymerization of Cyclic Esters

Wei-Han Rao, Lin Yu, and Jian-Dong Ding*

*State Key Laboratory of Molecular Engineering of Polymers, Department of Macromolecular Science, Fudan University, Shanghai 200438, China*

Electronic Supplementary Information

**Abstract** Coordination-insertion ring-opening polymerization (ROP) of cyclic esters is an industrial way to synthesize polyesters, which are widely applied in biomedical and environment-benign fields. However, the rate-determining transition state (TS) identified by the conventional reaction pathways (pathway A and pathway B) presented in the literature did not well describe the structure-reactivity relationship. The misidentification of the rate-determining TS might arise from the less ergodicity in the search of reaction pathways. Herein, we suggested a stride strategy based on the insight that even a partial double bond is rotatable at the catalysis temperature. As a result, we revealed a new reaction pathway, pathway C with a torsion transition state TSC2, by density functional theory (DFT). We also carried out kinetic experiments of ROP of D-lactide (D-LA), L-lactide (L-LA), ε-caprolactone (CL), and δ-valerolactone (VL), using poly(ethylene glycol) as the initiator and stannous octoate as the catalyst. The excellent linearity between the calculated free energy barriers and logarithms of the experimental kinetic constants of the two kinds of lactide and lactone monomers, was established, validating the quasi-ergodic search of reaction pathways and the scaling predicted by transition state theory. The linearity was highly predictive for the other lactide and lactone monomers, demonstrated by glycolide (GA) and trimethylene urethane (TU).

**Keywords** Coordination-insertion mechanism; Ring-opening polymerization; Density functional theory; Biodegradable polymer; Lactide; Lactone; Cyclic ester

**Citation:** Rao, W. H.; Yu, L.; Ding, J. D. Stride strategy to enable a quasi-ergodic search of reaction pathways demonstrated by ring-opening polymerization of cyclic esters. *Chinese J. Polym. Sci.* **2023**, *41*, 745–759.

## INTRODUCTION

Aliphatic polyesters, a class of important polymers with sustainability, biodegradability and biocompatibility,[1–7] are usually synthesized *via* ring-opening polymerization (ROP) of cyclic esters.[8,9] Many ROP reactions proceed through coordination insertion.[10–14] While a series of metal ions (*e.g.*, main group metals, transition metals, and rare earth metals) can be used as the active center of catalyst,[15–17] $Sn^{2+}$ has been used in industry for ROP and is thus particularly useful. A large number of catalyst/initiator combinations have been tried,[18–20] and the initiators for the coordination-insertion ROP are usually with at least one amino or hydroxyl terminal, for instance poly(ethylene glycol) (PEG) with hydroxy end groups.[21–25] However, even if more and more cyclic ester monomers are applicable for ROP,[26–29] a satisfactory theoretical structure-reactivity relationship between catalyst/initiator combinations and polymerizable monomers is still absent. Thus, comprehensive fundamental research of coordination-insertion ROP of cyclic esters triggered by a complex of catalyst and initiator is much required.

Transition state (TS) theory, which was published independently by Eyring[30] and Ewans-Polanyi[31] both in 1935, is one of the most useful chemical theories.[32] Under the framework of TS theory, the activity of a multistep reaction is regulated critically by the corresponding rate-determining TS, namely the highest saddle point on the potential energy surface (PES), along the so-called reaction coordinate. The calculated energy barriers of rate-determining TSs in a theoretical study are, in principle, linearly correlated with logarithms of the reaction rate constants obtained from experiments according to Eyring-Polanyi equation in TS theory expressed as follows:

$$k = \frac{k_B T}{h} e^{-\Delta G/RT} \quad (1)$$

where $k_B$ is Boltzmann constant, $h$ is Planck constant, $T$ is absolute temperature, $R$ is ideal gas constant, and $\Delta G$ is free energy barrier in the unit of kcal·mol$^{-1}$. Given the well-established linear relation of a reaction system, the reaction rate constants of subsystems can be predicted by the calculated energy barrier. Then the key to a multistep reaction is to identify the real rate-determining TS with the globally minimum energy barrier. Since reaction dynamics is complicated,[33] much

* Corresponding author, E-mail: jdding1@fudan.edu.cn

Special Issue: In Memory of Professor Fosong Wang
Received November 30, 2022; Accepted December 25, 2022; Published online February 21, 2023

progress has been made in identifying rate-determining TS and pertinent modelling of a chemical reaction.[34–38] Density functional theory (DFT) has revolutionized the studies of reaction mechanisms by providing a significantly more cost-effective way to predict the configuration or conformation of a TS and calculate the corresponding energy barrier of the TS during a reaction process.[39] However, despite the efforts of many researchers in DFT modelling, the linear relation in a large range has not been well established in the literature of coordination-insertion ROP, although valuable efforts have been made in a small range.[40,41] We surmised that the previous researches of coordination-insertion mechanism omit some key dynamic steps and the corresponding reaction pathways, making the less ergodicity of reaction pathway search. As a result, the predictability of the theoretical calculations is limited.

It is worthy of noting that the quantum chemistry in finding a rate-determining TS of a multistep reaction is, different from those more coarse-grained modellings such as molecular dynamic simulation and dynamic Monte Carlo simulations in other microscopic modelling of chain dynamics,[42–49] not able to proceed through an automatic ergodic search, because of the very high dimensions of PES. A predicted rate-determining TS with the energy barrier is always accompanied with a hypothesized reaction pathway instead of a global search on PES. The resulting less ergodicity makes the obtained rate-determining TS highly dependent upon experiences, which might be the bottleneck in identifying the real rate-determining TS with the globally minimum energy barrier in a multistep reaction.

To solve this problem, we supposed a stride strategy to enable a quasi-ergodic search of reaction pathways. While the conventional small step search probably afford the TSs and the corresponding pathways fettered in the local landscape, the "stride" mentioned here starts with a conscious and bold try beyond the tradition to discover the new reaction pathways to enable a quasi-ergodic search and help identify the real rate-determining TS. As schematically presented in Fig. S1 (in the electronic supplementary information, ESI), the final question might be how to achieve an appropriate stride. The present study is aimed to report this strategy with the important ROP of cyclic esters as demonstration.

The most popular way to synthesize biodegradable polyester is coordination-insertion ROP of cyclic esters using PEG as initiator and stannous octoate ($Sn(Oct)_2$) as catalyst.[50,51] The classic procedure[52–55] is named as pathway A here. As shown in Fig. 1, pathway A involves two transition states starting with the carbonyl-oxygen coordinated complex of trigger and monomer; after the transition state 1 following the nucleophilic attack in pathway A (TSA1), the ester bond outside the ring is formed in intermediate state 1 (IntA1); prior to the transition state of ring-opening (TSA2), a transformation from IntA1 to IntA2 proceeds because the coordination of the ester oxygen in the ring to the tin ion is necessary for the disruption of the intra-ring ester bond; finally, the reacted monomer inserts into the Sn—O bond of the trigger through TSA2 to afford the ROP product. Pathway B is a more direct

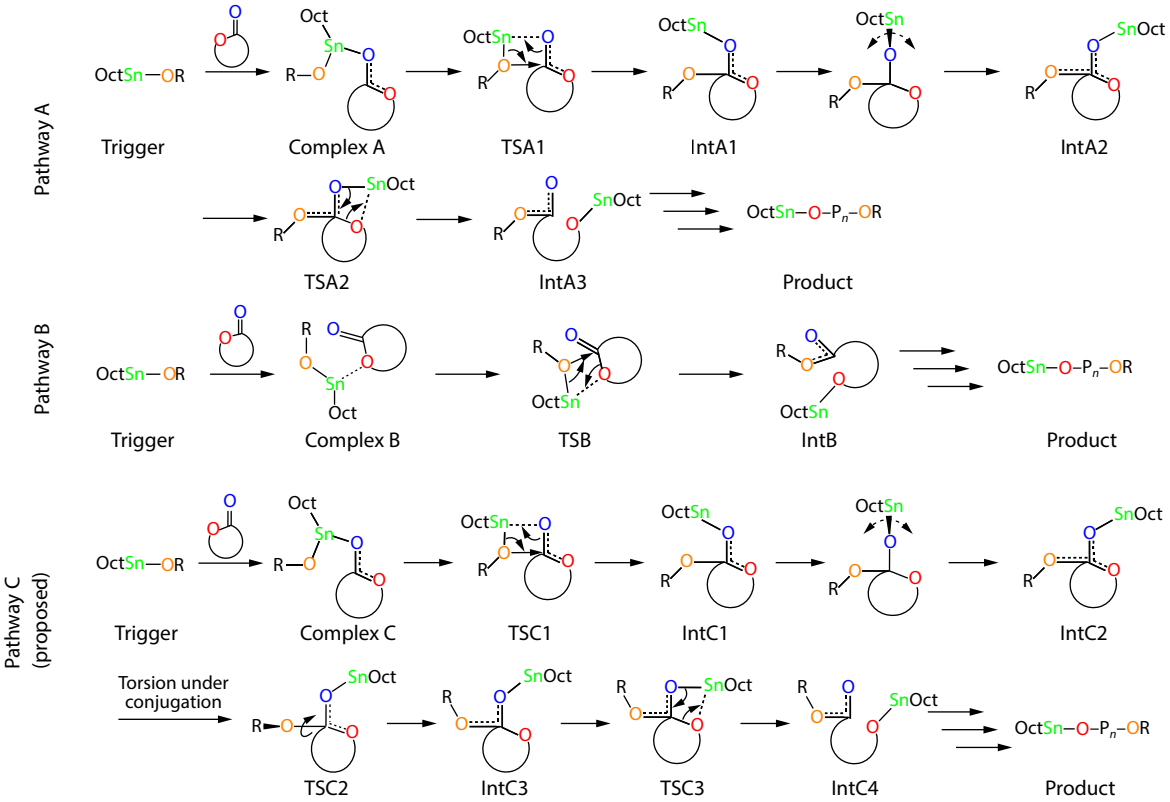


**Fig. 1** Reaction pathways of the coordination-insertion ROP of cyclic esters. Pathway A involves two transition states (TSA1 and TSA2) after the coordination of the carbonyl oxygen to Sn, and pathway B contains only one transition state after the coordination of the ester oxygen to Sn. The pathway proposed for the first time in this work (named pathway C) distinguishes itself mostly by the torsion transition state TSC2.

https://doi.org/10.1007/s10118-023-2930-6

one, in which the ring is opened through the corresponding ring-opening transition state (TSB) characterized by the ester oxygen to the tin ion. However, the search only involving pathway A and pathway B cannot well describe the due linear relation between free energy barrier and the logarithm of reaction constant, which will be presented in Discussion of this publication.

Herein, we adopted a "stride" and discovered a new reaction pathway (named as pathway C) to involve a torsion transition state TSC2 of the ester bond outside the ring. The consequent another new ring-opening transition state TSC3, was added, and a quasi-ergodic reaction pathway search of coordination-insertion ROP is enabled for the first time. Six kinds of monomers, D-lactide (D-LA), L-lactide (L-LA), $\varepsilon$-caprolactone (CL), $\delta$-valerolactone (VL), glycolide (GA), and trimethylene urethane (TU), were investigated in the formulism of the quasi-ergodic search among all three reaction pathways of ROP, using the methodology of DFT modelling. Combined with the kinetic experiments of ROP of the indicated monomers, the highly linear relationship between the calculated energy barriers and logarithms of the experimental rate constants was established among D-LA, L-LA, CL, and VL. The established relationship works in a wide range and its extrapolatablity for both lactide and lactone monomers was confirmed by dealing with other two kinds of monomers (GA and TU). This excellent structure-reactivity relationship has validated the identification of the real rate-determining TSs of coordination-insertion ROP and the corresponding ergodicity of the search of reaction pathways after adding pathway C, which was achieved by the appropriate stride strategy suggested in this work.

## EXPERIMENTAL

### Kinetic Experiments

Bulk polymerization was carried out by ring-opening of cyclic esters under the nitrogen atmosphere. Monomers and the initiator PEG1500 were transferred into the annealed glass vessels in bulk. The catalyst $Sn(Oct)_2$ in toluene solution was distributed into the reaction system. A typical polymerization process was performed at 140 °C for 1 h using standard Schlenk techniques, and the sampling samples were quenched by cooling down rapidly. $^1$H-NMR and GPC were utilized to characterize the polymerization products and kinetic samples to obtain the number-average molecular weight ($M_n$) of (co)polymers and molar mass dispersity. Details can be seen in Supplementary Methods in ESI.

### DFT Calculations

DFT was used to model the key reaction states on the atomic level and the truncated models of the corresponding triggers as shown in Fig. 2 were adopted to accelerate the calculations. All geometry optimizations were performed in gas phase using the M06-2X functional,[56] a hybrid meta-GGA functional with high accuracy in computing energy barriers[57] with the empirical D3

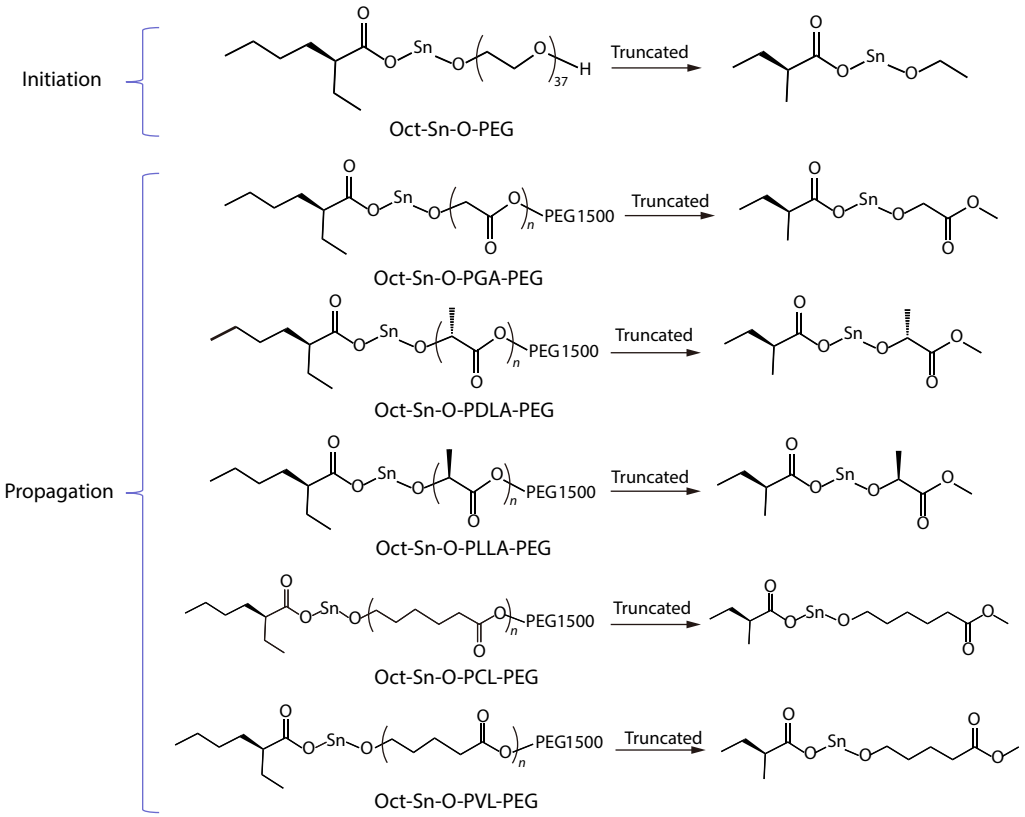


**Fig. 2** The truncated triggers involved in the DFT calculations. PGA is the polymerization product of glycolide (GA), PDLA is the product of D-lactide (D-LA), PLLA is the product of L-lactide (L-LA), PCL is the product of $\varepsilon$-caprolactone (CL), and PVL is the product of $\delta$-valerolactone (VL). The polymerization product of trimethylene urethane (TU) is absent since the propagation of TU is undetectable in the experimental time.

https://doi.org/10.1007/s10118-023-2930-6

long-range-dispersion correction established by Grimme *et al*.[58] The basis set employed for all atoms in geometry optimization and frequency analysis was Def2-TZVP.[59] All calculations were performed using the Gaussian 09 software package[60] with the assistance of Molclus program[61] in rigid scan. Default self-consistent field, ultrafine integral lattice, and tight geometry optimization convergence criteria were used in the calculations.

## RESULTS

### Rationality of the Stride and thus Feasibility of Pathway C

The "stride" suggested in this study of ROP comes from the rotation of a partially conjugated ester bond. Before the occurrence of this stride, the reaction system experiences the formation of complex C, intermediate C1 (intC1) and intermediate C2 (intC2), as schematically presented in Fig. 1. Pathway C proceeds through the same transformation from Int1 to Int2 with pathway A. We first justify the rationality of the transformation from intC1 to intC2, namely, a free swing around carbonyl bond. Here, the term "free" does not necessarily mean no energy barrier, but means not a rate-determining TS under the normal experimental condition. The swing around carbonyl bond has been regarded as a free process in some reports,[62–66] while some other researchers considered it as a candidate of rate-determining TS.[67] To confirm the rationality of the transformation process, we examined a swing transition state using DFT by adopting the initiation stage of CL as a model. According to the three-dimensional (3D) demonstration of the transformation in Fig. S2 (in ESI), this process can be analogous to a side somersault of the $Sn(Oct)_2$ residue, and the corresponding intrinsic reaction coordinate (IRC) plots is shown in Fig. S3 (in ESI). The swing transition state in the local energy profile of pathway A or pathway C (Fig. S4 in ESI) was far away from being a rate-determining TS of the reaction pathway. So the swing can be regarded as "free".

The key new input of the stride suggested here comes from the rotatability of the partially conjugated ester bond from intC2 to intermediate C3 (intC3), and pathway C thus works on the rationality of the torsion transition state of the ester bond outside the ring. The molecular structures of important Ints and TSs in the reaction pathway of ROP of cyclic esters contain two ester bonds sharing the same carbonyl group. It is well-known that an ester bond is a partially conjugated bond. With the common knowledge of the non-rotatability of a normal double bond, the rotation of a conjugated double bond seemed to lie on a vague zone. Therefore, we first conducted a validation of the suggested stride—the rotation of an ester bond—by combining theoretical calculation with experiments.

As demonstration, we carried out first the rigid scans of the corresponding chemical bonds (carbon-carbon double bond, carbon-nitrogen conjugated double bond, carbon-oxygen conjugated double bond, and carbon-carbon single bond) of the four kinds of model molecules, ethylene, *N*,*N*-dimethylacetamide (DMA), methyl acetate, and ethane. The DFT results are shown in Fig. S5 and Table S1 (in ESI). The resultant energy barriers of the rotation of the two conjugated double bonds were far away from that of the normal carbon-carbon double bond, which implies the possibility of rotation of the conjugated double bonds.

We performed more quantitative DFT calculations for the rotation process of the two conjugated bonds at the theoretical level of M06-2X/Def2-TZVP. The IRC plots are shown in Fig. S6 (in ESI), and the free energy barriers are listed in Table S2 (in ESI), giving 18 and 13 kcal·mol$^{-1}$ for the amide conjugated double bond and the ester conjugated double bond at 25 °C, respectively. The rotation rates of these two conjugated bonds can be estimated through transition state theory by considering the rotation process as a monomolecular reaction. As shown in Table S3 (in ESI), the boundary between a rotational process and an unrotational process lies between 20 and 21 kcal·mol$^{-1}$ energy barriers. Therefore the 13 kcal·mol$^{-1}$ barrier in the rotation process of an ester bond could be completely neglected under a normal detection.

Furthermore, we conducted the $^1$H-NMR tests of DMA and methyl acetate at a series of temperatures to confirm the rotation probabilities of the partial conjugated double bonds experimentally. As shown in Fig. 3(a), the transformations

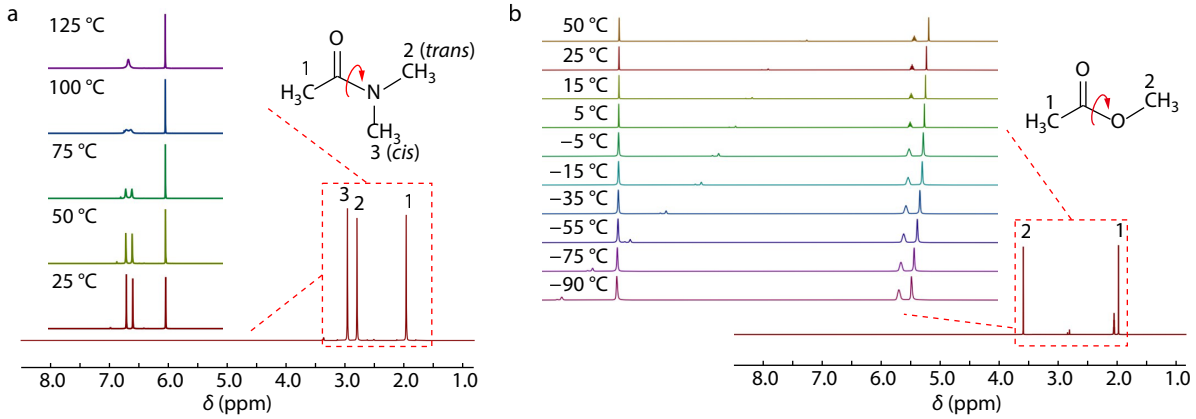


**Fig. 3** Variable-temperature $^1$H-NMR spectra of DMA in DMSO-$d_6$ and methyl acetate in acetone-$d_6$. (a) The well-separated signals of the two *N*-methyl in DMA gradually merge with the increase of temperature, indicating the acceleration of the rotation of the conjugated C—N bond. The transition occurred in the temperature range from 100 °C to 125 °C. (b) No significant change of the signals of the two methyl groups in methyl acetate is observed from −90 °C to 50 °C.

https://doi.org/10.1007/s10118-023-2930-6

from bimodal peaks (assigned as the signals of *trans* and *cis* *N*-methyl groups) to a unimodal peak occurred between 100–125 °C in DMA, indicating the rotatability of the amide bond.

The comparative DFT studies between DMA and methyl acetate illustrates that the rotation transition occurs at temperature between −5 and 5°C, as listed in Table S4 (in ESI). According to Fig. 3(b), no significant change was observed in the $^1$H-NMR tests of methyl acetate in the temperature range from −90 °C to 50 °C in acetone-$d_6$. The tests in $CDCl_3$ in the temperature range from −60 °C to 50 °C were also conducted, and the results are shown in Fig. S7 (in ESI). There is an overwhelming population of *trans*-methyl acetate to *cis* methyl acetate even at 50 °C, according to our calculational results of the ratio of *trans* population collected in Table S5 (in ESI). That is why DMA was employed as one of model molecules in the NMR experiments. In this case, two methyl groups are linked to the amide bond, which guarantees the equal population of the *cis* and *trans* methyl groups and thus sufficient NMR signals to distinguish both of them.

The combination of the above varied-temperature $^1$H-NMR results and DFT calculations illustrated the rotatability of an ester bond at reaction temperature. The rotation of the C—N conjugated bond in DMA with a significantly higher energy barrier than the ester bond in methyl acetate was free below the reaction temperature 140 °C of the ROP process of cyclic esters, and the ester bond is rotatable even at room temperature (RT), as illustrated in Table S4 (in ESI).

## DFT Calculations of Pathway C Demonstrated by CL Initiation

Four typical chemical bonds are shown in Fig. 4(a) to represent the extent of rotatability. The fast rotation of the ester bond at room temperature grants the stride legitimacy at the normal

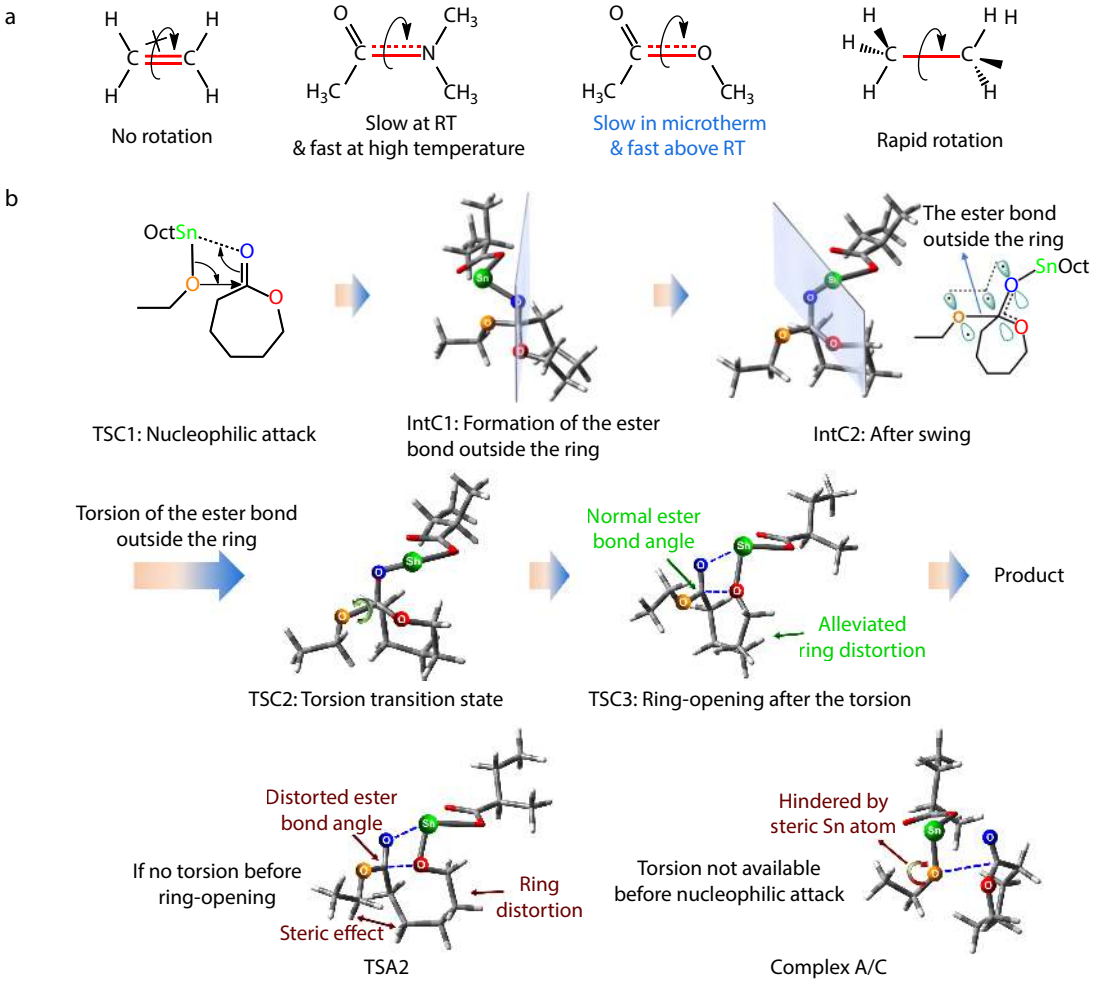


**Fig. 4** The new pathway proposed in this work using CL initiation as a demonstration. (a) Schematic presentation of rotatability of a conjugated ester bond at normal experimental condition in comparison with three other typical bonds. (b) Representative structures form our DFT calculations to illustrate significance of the torsion transition state TSC2 of the ester bond outside the ring. Pathway C starts with a nucleophilic attack; after the transformation from IntC1 to IntC2 (the plane determined by the three atoms of the ester bond in the ring shows the change of spatial relative position through the transformation), the ring-opening step is able to occur with the conjugation of the ester bond outside the ring. If ring-opening follows the torsion transition state TSC2 of the ester bond outside the ring, a less structural distortion of ring-opening transition state can be afforded. If no torsion occurs before, ring-opening step would suffer from the distorted bond angle of the ester bond outside the ring and the distorted ring structure, and steric effect between RO group and ring. Besides, torsion is not available before nucleophilic attack owing to the steric effect of the Sn atom.

https://doi.org/10.1007/s10118-023-2930-6

reaction temperature of coordination-insertion ROP of cyclic esters. The stride made the key configurations during pathway C with the torsion transition state TSC2 of the ester bond outside the ring and the corresponding significance of TSC2 exposed to our vision, as demonstrated by CL initiation (Fig. 4b).

We mapped out the free energy profile and the bond length changes of the two ester bonds along with the reaction coordinate of pathway C in the case of CL initiation. According to Fig. 5, a decrease in bond length of the ester bond outside the ring and an increase in bond length of the ester bond in the ring indicate the competition of the two ester bonds along the reaction process even though the carbonyl carbon is seemingly a tetra-single-bonded one, resulting in the formation of a linear ester bond and the disruption of a cyclic ester bond along with the ring-opening process. The corresponding changes in the bond angles of the two ester bonds can be seen in Figs. S8 and S9 (in ESI). The free energy barrier of the ring-opening transition state TSC3 through TSC2 is lower than that of TSA2, making TSC1 stand out as a top contender of the rate-determining step of coordination-insertion ROP of cyclic esters.

We also examined the effects of spatial positions between trigger and monomer during the early coordination between Sn (in catalyst) and O (in monomer) on the free energy of the later transition state. Fig. 6 shows four spatial types for TSC1. Different types of TSC1 lead to different types of TSC2 and TSC3, but only two types were defined for TSC2 and TSC3 since *trans* and *cis* afford the same configuration after the transformation from IntC1 to IntC2. The outside-*trans* initial configuration of the reactant complex afforded the minimum free energy barrier of pathway C in the case of the ROP of CL initiated with PEG and catalyzed with $Sn(Oct)_2$.

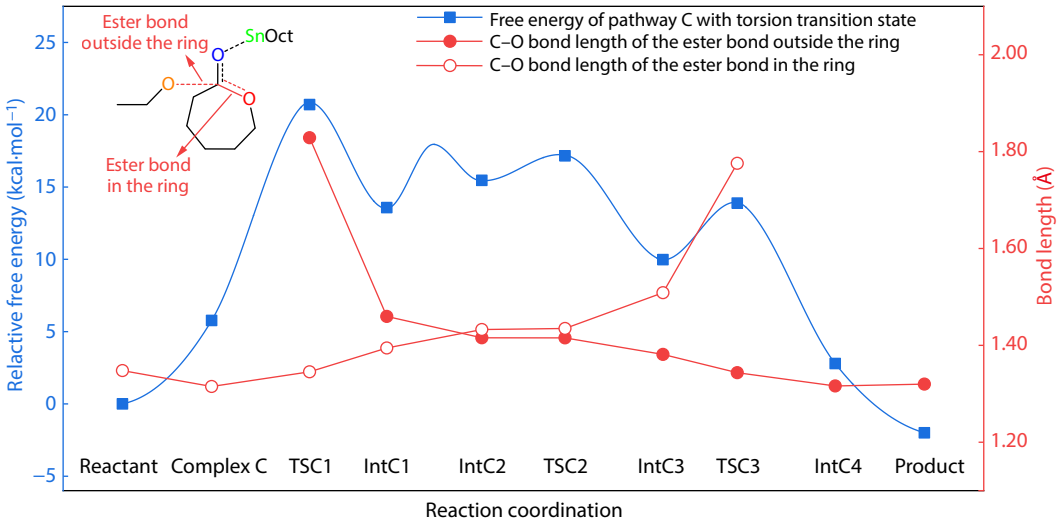


**Fig. 5** Bond length changes of ester bonds and free energy profile along with the reaction coordinate of pathway C in the case of CL initiation.

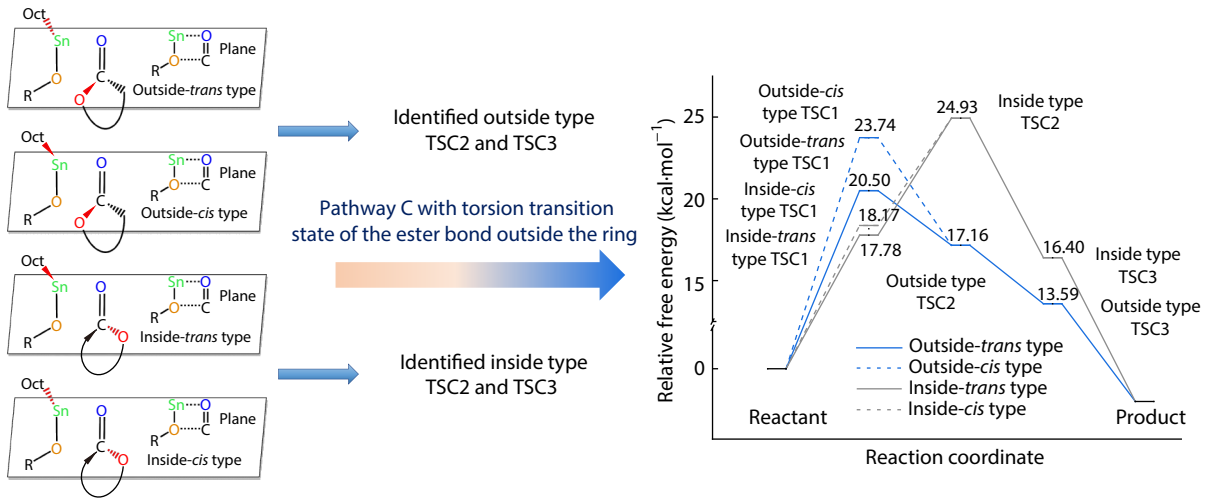


**Fig. 6** The effects of spatial types on free energies in pathway C. Four types (named outside-*trans* type, outside-*cis* type, inside-*trans* type, and inside-*cis* type) are defined for TSC1, where outside or inside means that the ester oxygen in monomer is on the outside or inside of the reference plane, respectively, and *trans* or *cis* means that the isooctyl ligand and the ester oxygen are on the same side or on the opposite side of the reference plane, respectively. The spatial type has a significant effect on the energy profile of pathway C, and one of the four types should be optimal through pathway C.

https://doi.org/10.1007/s10118-023-2930-6

### Combination of Quasi-ergodic Search of Reaction Pathways and Kinetic Experiments Using CL as a Demonstration

The quasi-ergodic search of reaction pathways in this work was conducted using the methodology of DFT modelling. The ROP of cyclic esters involves a chain initiation stage (namely the first insertion of monomers) and the followed propagation stage.[68–71] The change of chemical structures of triggers along with polymerization processes are schematically presented in Fig. S10 (in ESI).

We calculated all pathways in Fig. 1 with the spatial types defined in Fig. 6 for both initiation and propagation stages using DFT at the theoretical level of M06-2X/Def2-TZVP. The optimal energy barriers of three pathways in Fig. 7 illustrate the superiority of pathway C with the torsion transition state TSC2 to other pathways in both initiation and propagation

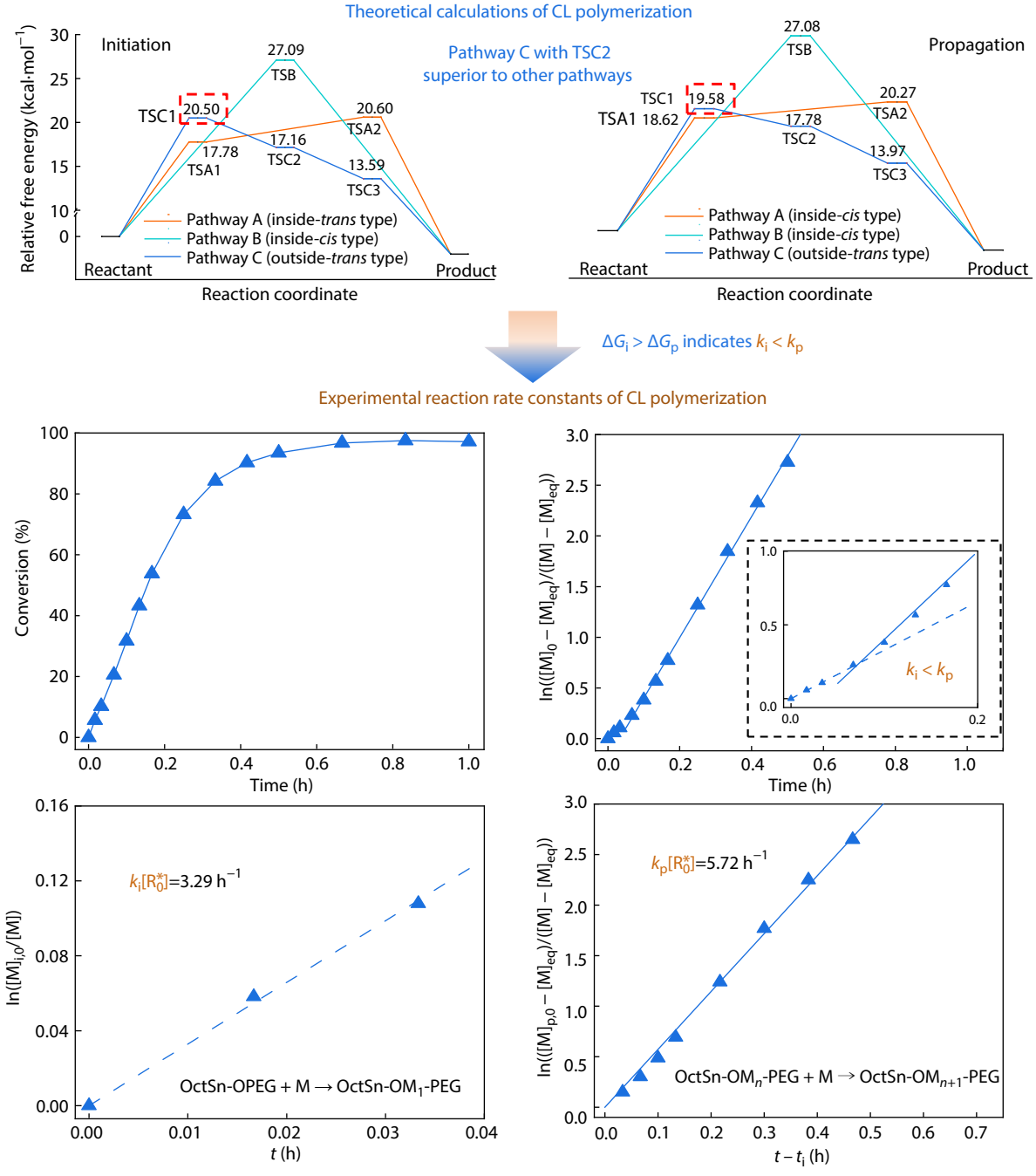


**Fig. 7** The calculation results of pathway C obtained from DFT and the experimental kinetics results of the bulk polymerization, using CL as a demonstration. The experiment was performed under the 1/50 molar ratio of catalyst/initiator. For pathways A, B and C, only the results with respect to the corresponding optimal initial spatial types are presented. The kinetic experiment of CL confirms the calculation results and gives the experimental reaction rate constants of initiation and propagation with $R^2$=0.9949 according to Eq. (1) and $R^2$=0.9985 according to Eq. (3).

https://doi.org/10.1007/s10118-023-2930-6

stages. The rate-determining TSs of initiation and propagation of CL were both the corresponding outside-*trans* types of TSC1, but different free energy barriers (20.50 kcal·mol$^{-1}$ for initiation and 19.58 kcal·mol$^{-1}$ for propagation) were given, indicating the higher experimental reactivity of propagation of CL than initiation.

A theoretical energy barrier of a real rate-determining TS should be reflected from the corresponding experimental kinetics. To confirm the obtained theoretical results, we conducted the kinetic experiment of CL, in which the experimental reaction rate constants of the initiation stage and the propagation stage were calculated based on the following equations:

$$k_i\left[R_0^*\right]t = \ln\left(\frac{[M]_{i,0}}{[M]}\right), 0 \le t \le t_i \quad (2)$$

$$k_p\left[R_0^*\right](t - t_i) = \ln\left(\frac{[M]_{p,0} - [M]_{eq}}{[M] - [M]_{eq}}\right), t > t_i \quad (3)$$

where $k$ is reaction rate constant, $\left[R_0^*\right]$ is initial concentration of trigger, $t$ is time, $t_i$ is the reaction time of initiation step, $[M]$ is concentration of monomer, and subscripts "i" and "p" mean initiation and propagation, respectively. The detailed derivation along with Eqs. S(1) and S(2) are given in ESI. The experimental plots of conversion versus time and corresponding kinetic fittings are shown in Fig. 7. The data confirmed the higher reactivity of the propagation stage of CL than the initiation stage.

## The Universality of the Quasi-ergodic Search Enabled by the Stride Strategy

We investigated other five kinds of monomers in both initiation and propagation stages to further verify the rate-determining TSs after combination of DFT calculations of all three pathways with kinetic experiments. Figs. S11 and S12 (in ESI) indicate that, at the initiation stage, TSC1 of pathway C is the rate-determining TS in the cases of GA, D-LA, L-LA, CL, and VL, while TSC2 of pathway C is the rate-determining TS in the case of TU; at the propagation stage, TSC1 of pathway C is the rate-determining TS in the cases of D-LA, L-LA, CL, and VL, while TSC2 of pathway C is the rate-determining TS in the case of GA. Although pathway C is always superior to both pathways A and B (see Tables S6 and S7 in ESI for more details), pathway A is competitive in the cases of CL initiation and VL initiation, indicating the very significance of the quasi-ergodic search of reaction pathways.

It should be noticed that the optimal spatial types are dependent upon monomers, pathways, and reaction stages, suggesting the necessity of considering the effect of the initial spatial type on the energy profile of the forthcoming reaction, which might also be another quasi-ergodic search in a sense. The optimal energy profiles of the indicated monomers are mapped out in Fig. 8(a), and the corresponding rate-determining TSs are highlighted by the dashed cycles and the energy barrier values. D-LA and L-LA exhibited equivalent ROP reactivities at both initiation and propagation stages, and CL exhibited equivalent reactivity to VL only at the initiation stage.

To validate the rate-determining TSs identified by the quasi-ergodic search of reaction pathways. The experimental kinetic constants of initiation and propagation stages of D-LA, L-LA, and VL were determined by the same procedure as CL. The polymerization results together with those of CL are presented in Fig. 8(b). More details of concentration and conversion of monomers with reaction time are presented in Fig. S13 (in ESI). The corresponding NMR spectra and gel permeation chromatography (GPC) profiles of the synthesized copolymers are shown in Figs. S14–S22 (in ESI). The ROP of D-LA and L-LA proceeded in almost the same reaction rate at both initiation and propagation stages while the initiation plots of CL almost coincided with those of VL, indicating the validity of the calculation results qualitatively.

The main results of the six kinds of monomers obtained by DFT calculations and direct experimental kinetic fitting were collected in Fig. 8(c) with three "NA"s indicating the absence of the experimental data, which we have to obtain through indirect methods as follows.

## The Indirect Experimental Methods to Obtain the Reaction Constants Not Available in the Normal Kinetic Experiments

Obtaining the constants hard to gain in the normal kinetic experiments is of interest for validating the power of the quasi-ergodic search of reaction pathways enabled by the stride strategy. We employed the copolymerization of GA and L-LA to estimate the reaction constant of GA, namely $k_{GA}$, based on that of L-LA $k_{L\text{-}LA}$ from the homopolymerization of L-LA and the ratio between them $k_{GA}/k_{L\text{-}LA}$ from the copolymerization calculated with Eq. S(1) (in ESI). The basic idea is summarized in Fig. S23 (in ESI). Set the initial concentration of trigger as $\left[R_0^*\right]$, one can obtain $k_{GA}\left[R_0^*\right]$ by Eq. S(2) (in ESI). The copolymerization of GA and L-LA with equimolar feeding can significantly impede the otherwise crystallization of PGA during homopolymerization of GA. The copolymerization process of GA and L-LA was detected with $^1$H-NMR, and some typical spectra are presented in Fig. S24 (in ESI). As summarized in Fig. S25 (in ESI), $k_{i,GA}\left[R_0^*\right] = 95.51$ h$^{-1}$ and $k_{p,GA}\left[R_0^*\right] = 63.21$ h$^{-1}$ for the initiation and propagation stages of GA, respectively.

The issue of TU is different with GA. In principle, its polymerization product PTU prefers to depolymerization. The free energies of the assumed reactant and product are shown in Fig. S26 (in ESI). The complex consisting of the trigger and TU monomer afforded a lower free energy than the product after introducing the interaction of N—H···O hydrogen bond, indicating a thermodynamically unsupported process of polymerization of TU, which is consistent with our experiment (for instance, the GPC profiles of the samples in the presence of the initiator PEG 1500 at different reaction times in Fig. S27 in ESI) and also with the depolymerization of PTU with Tin-based catalyst at 140 °C reported by Neffgen *et al*.[72] Nevertheless, it does not mean that the very initiation cannot occur. The calculated energy barrier of 30.03 kcal·mol$^{-1}$ in Fig. 8(c) was less than the empirical 35 kcal·mol$^{-1}$ for a feasible reaction, which suggested a detectable reactivity of TU initiation at 140 °C. To validate this, we performed a series of NMR measurements till 48 h and the spectra are shown in Fig. S28 (in ESI). About 1.5% conversion was detected at 1 h, while the conversion of TU upon linking each hydroxy end of the initiator PEG1500 with

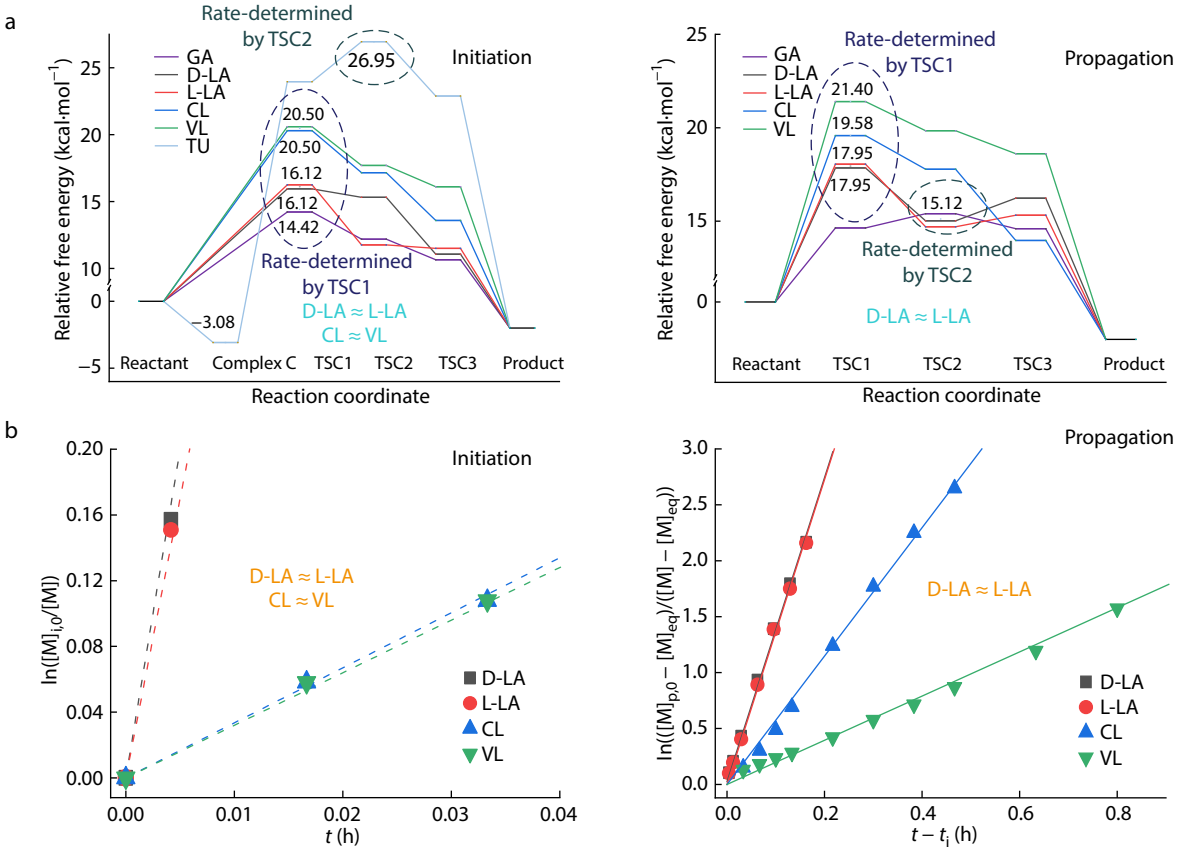


c

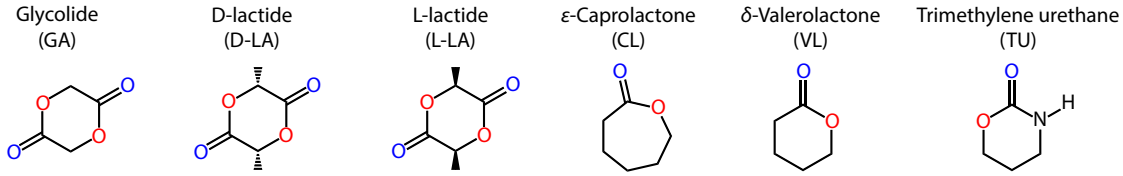


| Monomer | Rate-determined step of initiation | $\Delta G_i$ (kcal/mol) | $k_i[R_0^*]$ ($h^{-1}$) | Rate-determined step of propagation | $\Delta G_p$ (kcal/mol) | $k_p[R_0^*]$ ($h^{-1}$) |
|---|---|---|---|---|---|---|
| GA | TSC1 | 14.42 | NA [a] | TSC2 | 15.12 | NA [a] |
| D-LA | TSC1 | 16.12 | 37.67 | TSC1 | 17.95 | 13.83 |
| L-LA | TSC1 | 16.12 | 36.21 | TSC1 | 17.95 | 13.63 |
| CL | TSC1 | 20.50 | 3.29 | TSC1 | 19.58 | 5.72 |
| VL | TSC1 | 20.50 | 3.29 | TSC1 | 21.40 | 1.97 |
| TU | TSC2 | 30.03 | NA [b] | | NA [c] | |

**Fig. 8** DFT calculational outputs and the experimental results of ring-opening polymerization of different monomers. (a) The optimal free energy profiles from DFT calculations of ROP of the indicated monomers. Only TSC1 and TSC2 in pathway C are candidates for rate-determining TS, which affords the calculated energy barriers of coordination-insertion ring-opening polymerizations of monomers investigated in this work. The values indicate the relative energies of the rate-determining TSs of ROP of the corresponding monomers. (b) The kinetic fitting of the initiation stage and the propagation stage of monomers except GA and TU. The experiments were performed under the 1/50 molar ratio of catalyst/initiator with the same mass feeding of initiator and monomers, respectively. The result of GA is absent because the initiation stage of GA was too fast to monitor and the kinetic characteristics of the propagation stage of GA is supposed to be disturbed by the crystallization of PGA. The result of TU is absent because only 1% conversion was observed in reaction time, which disabled the kinetic fitting under the same condition with other monomers. The fitting lines of D-LA and L-LA, CL and VL, in initiation are almost coincident, and the closed dashed lines were separated slightly to highlight that the number of fitting lines is four. (c) The collection of main results obtained by calculations and experimental kinetic fittings investigated in this work. Rate-determined TSs were identified by the quasi-ergodic search of all three pathways, although pathway C was always the most favored one. Subscripts "i" and "p" mean the initiation and propagation stages, respectively. "NA [a]" means the data was not available because the initiation of GA is too fast to be monitored and the propagation of GA is supposed to be disturbed significantly by the high crystallinity of PGA even in a low $M_n$; "NA [b]" means the data was not available because no significant initiation was observed in the time scale of the kinetic experiments; "NA [c]" means the calculation is not meaningful because of the absence of experimental propagation of TU.

https://doi.org/10.1007/s10118-023-2930-6

one ring-opened monomer reads 6.7%. As indicated by Fig. S29 (in ESI), the increase of the conversion after 1 h was extremely low, indicative of the depolymerization after the very initial ROP.

So it is interesting that the initiation of the first monomer might be followed by depolymerization for ROP of TU. Only the very initial data could be used to roughly estimate the initial reaction constant. As plotted in Fig. S30 (in ESI), $k_{i,TU}\left[R_0^*\right] = 0.0154h^{-1}$ based on the data in 1 h.

## DISCUSSION

Organic reactions including but not limited to polymerization play important roles in academic research and industry.[73–77] Most of them are accelerated by catalysts,[78–82] and thus understanding of the reaction mechanism is helpful for predicting the reactions.[83–86] While DFT has been widely used to study the catalysis process, it is rare to establish an extrapolatable relationship between theoretical energy and experimental constants, which is much required for a quantitative description of the reaction kinetics.[87–92] The difficulty is ever more significant in dealing with polymerization. With the development of biomedical materials,[93–98] biodegradable polymers such as aliphatic polyesters have been paid much attention, and the most important way to synthesize biodegradable polyester is ROP. Herein, we employed a stride strategy in the DFT investigation of the coordination-insertion mechanism of ROP of cyclic esters. Based on the stride to a new landscape, pathway C was added into and the corresponding quasi-ergodic search among three pathways revealed the regulation of a series of cyclic ester monomers.

### Establishing the Exponential Relationship or Linear Semilogarithmic Relationship

The theoretical results of the quasi-ergodic search are in agreement with the experimental ones. The exponential relationship or linear semilogarithmic relationship between experimental reaction rate constants and calculated energy barriers was established using the data collected in Fig. 8(c). If only pathway B was involved in identifying the rate-determining TS, the linear fitting resulted in qualitative error, as shown in Fig. 9(a), because of the very nonergodicity. The more ergodic search *via* pathways A and B resulted in a qualitatively correct

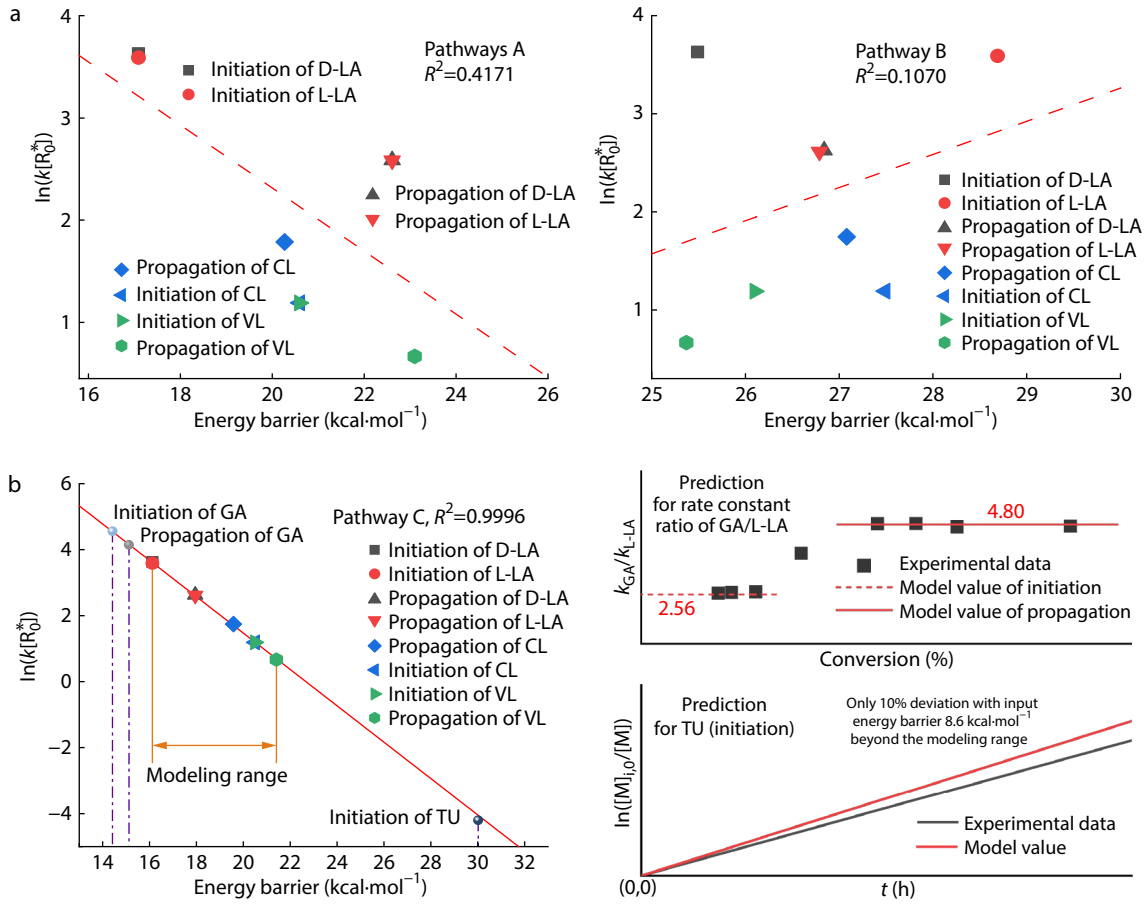


**Fig. 9** Comparison of the relationships between experimental reaction rate constants and calculated Gibbs free energy barriers established by different reaction pathway search. (a) The search only involving pathway B gave a qualitatively error result because of the positive slope. The search *via* pathway A or both pathways A and B gave a quantitatively poor correlation coefficient of determination. (b) A linear relationship, expressed as $Y = 12.554 - 0.554X$, between the semilogarithmic experimental reaction rate constants and the calculated Gibbs free energy barriers by the quasi-ergodic search *via* pathway C or *via* all three pathways was established with high goodness of fit. Model predictions for initiation and propagation of GA and initiation of TU were also presented.

https://doi.org/10.1007/s10118-023-2930-6

picture, yet a quantitatively worse linearity as comparison between Figs. 9(a) and 9(b). Hence, identifying the rate-determining TSs by a less ergodic way, namely without our stride to the new landscape to enlist the indispensable pathway C into the reaction pathway search, made the obtained energy barriers be the outliers of the fitting line.

The semilogarithmic relationship in Fig. 9(b) illustrates the excellent linear fitting of D-LA, L-LA, CL and VL. The data of GA and TU obtained by the indirect methods as depicted in Figs. S23–S25 and Figs. S26–S30 (in ESI) were plotted as well, which also match the established relationship. There are only slight deviations between the model values of rate constant ratio of GA/L-LA and the experimental data of copolymerization at both initiation and propagation stages. For the case of TU initiation with the input energy barrier 8.6 kcal·mol$^{-1}$ far beyond the modeling range, only 10% deviation between the model and experimental reaction rate constants was observed. Hence, the established relationship based on the quasi-ergodic search resulted in the excellent extrapolability.

## Understanding the Superiority of Pathway C

In order to understand how the landscape around TSC3 in pathway C possesses a significantly lower energy barrier than TSA2 in pathway A, we collected the bond lengths and the bond angles of the ester bond outside the ring in all cases of TSA2 and TSC3 investigated in this work into Tables S8 and S9 (in ESI) and plotted the bond lengths and the bond angles versus free energy barriers into Fig. 10.

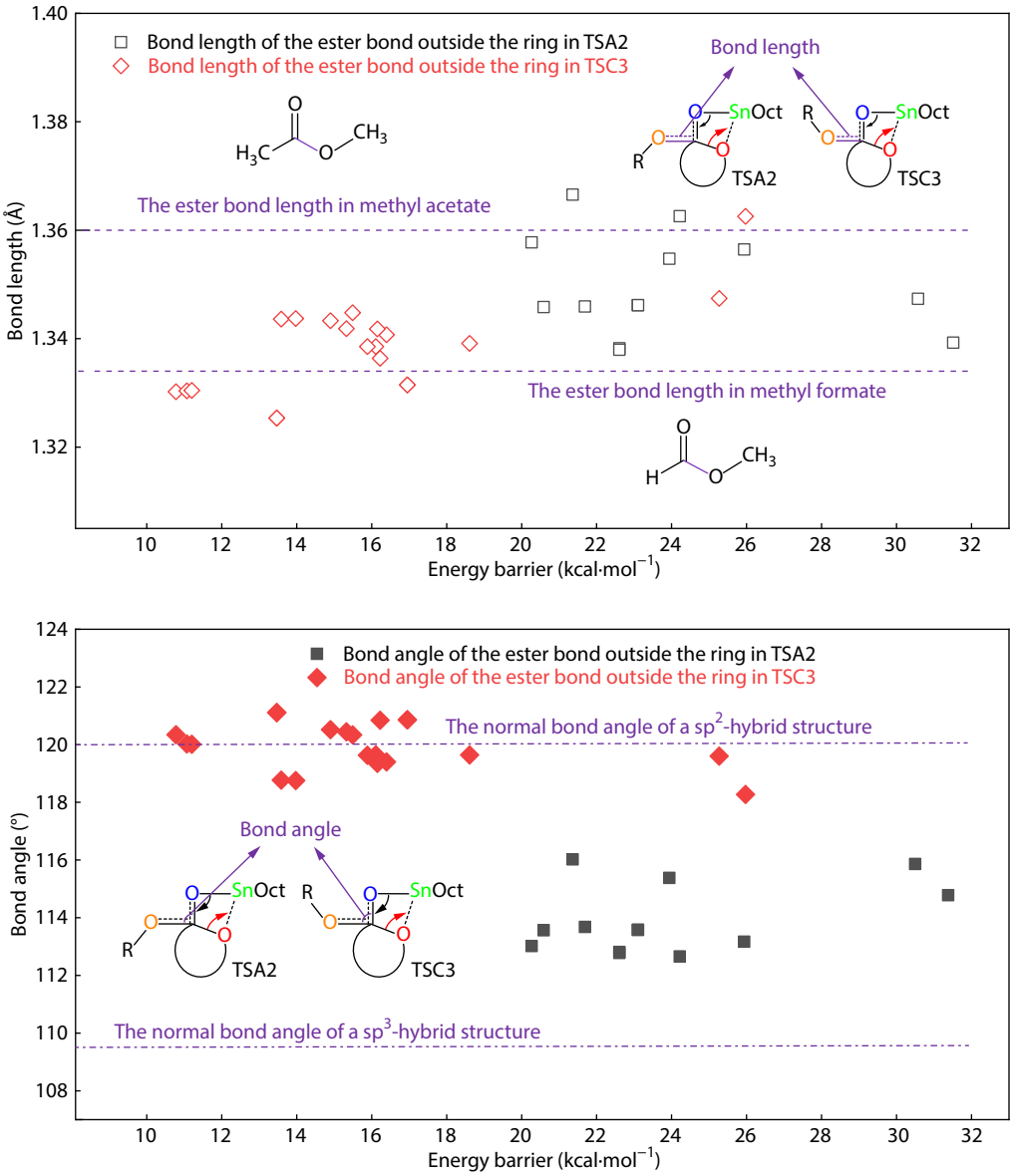


**Fig. 10** Correlation of bond lengths and bond angles of the ester bonds outside the ring to energy barriers of TSA2 and TSC3. The data are from six monomers with outside and inside type configurations of the transition states from DFT calculations. The bond lengths in TSC3 are closer to the ester bond length in methyl formate than those in TSA2, while the bond angles in TSC3 are significantly closer to the normal bond angle of a sp$^2$-hybridized structure than those in TSA2, indicating a stronger conjugation of the ester bond outside the ring in TSC3 than that in TSA2.

https://doi.org/10.1007/s10118-023-2930-6

It can be seen that the scatter points of the bond lengths in TSA2 are closer to the bond length of the ester bond in methyl acetate, while those in TSC3 are closer to the bond length of the ester bond in methyl formate. The shorter bond length of the ester bond outside the ring in TSC3 than TSA2 indicates a stronger conjugation in the ester bond outside the ring in TSC3 than TSA2. The bond angles in TSC3 reach the normal bond angle of a $sp^2$-hybridized structure while those in TSA2 are much closer to the normal bond angle of a $sp^3$-hybridized structure. We tried to calculate the average of all cases of TSC3 and TSA2, giving bond lengths 1.338 and 1.346 Å for TSC3 and TSA2, respectively, and bond angles 120.0° and 113.9° for TSC3 and TSA2, respectively. The lower energy barrier of TSC3 than TSA2 comes from the critical structure relaxation, which proceeds by the torsion transition state TSC2 based on the stride strategy suggested in this work.

Last, we would like to mention that according to our modelling (data not shown) of the ROP of lactam catalyzed by $Sn(Oct)_2$ is similar to that of TU initiation. We expect that the stride strategy in DFT calculations is powerful for dealing with other catalyst/initiator systems of ROP of cyclic esters and might be useful in mechanism studies of organometal-catalyzed polymerization of lactam.

## CONCLUSIONS

Ergodicity is a sufficient condition to obtain the global minimum barrier in mechanism research, which is still hard to achieve in quantum chemistry even if the methodology of DFT with higher cost-effectivity is applied. In this article, we suggested a stride strategy to enable a quasi-ergodic search of reaction pathways to identify the real rate-determining TSs. We tried this strategy to investigate the coordination-insertion mechanism of ROP of cyclic esters, of which a satisfactory structure-reactivity relationship is still absent in the literature. Based on the insight that even a partial double bond can be rotated at the catalysis temperature, a new pathway, named as pathway C, with the critical torsion transition state TSC2 of the ester bond outside the ring, was found.

The more ergodicity in reaction pathway search renders the linear semilogarithmic relationship between the experimental reaction rate constants and the calculated free energy barriers, using PEG and $Sn(Oct)_2$ as the model initiator and catalyst, respectively. The established relationship with high goodness of fit and excellent extrapolatability for both lactone and lactide monomers highlights the power of DFT calculations and *Eyring-Polanyi* transition state theory to predict catalysis reactions, and a prerequisite is the quasi-ergodicity of reaction pathway search to obtain the real rate-determining TSs. Hence the present study stimulates that in the case of unsatisfactory structure-reactivity relationship of a reaction series in DFT modelling, one can try a stride, namely, "unexpected on the surface" actions such as rotation of a partially conjugated chemical bond, leading to a relatively large scale and multi-atom displacement.

## NOTES

The authors declare no competing financial interest.

## Electronic Supplementary Information

Electronic supplementary information (ESI) is available free of charge in the online version of this article at http://doi.org/10.1007/s10118-023-2930-6.

## ACKNOWLEDGMENTS

The work was financially supported by the National Natural Science Foundation of China (No. 52130302). We thank Prof. Xin Xu, Prof. Zhenhua Li, and Prof. Junpo He for their critical reading of our manuscript.

## REFERENCES

1 Farah, S.; Anderson, D. G.; Langer, R. Physical and mechanical properties of PLA, and their functions in widespread applications—a comprehensive review. *Adv. Drug Deliv. Rev.* **2016**, *107*, 367–392.
2 Hillmyer, M. A.; Tolman, W. B. Aliphatic polyester block polymers: renewable, degradable, and sustainable. *Acc. Chem. Res.* **2014**, *47*, 2390–2396.
3 Ramot, Y.; Haim-Zada, M.; Domb, A. J.; Nyska, A. Biocompatibility and safety of PLA and its copolymers. *Adv. Drug Deliv. Rev.* **2016**, *107*, 153–162.
4 Yuan, Yin.; Shi, X. D.; Gan, Z. H. Wang, F. S. Modification of porous PLGA microspheres by poly-l-lysine for use as tissue engineering scaffolds. *Colloid. Surface B* **2018**, *161*, 162–168.
5 Cui, S. Q.; Yu, L.; Ding, J. D. Injectable thermogels based on block copolymers of appropriate amphiphilicity. *Acta Polymerica Sinica* (in Chinese) **2018**, 997–1015.
6 Tang, X.; Chen, E. Y. X. Toward infinitely recyclable plastics derived from renewable cyclic esters. *Chem* **2019**, *5*, 284–312.
7 Zhang, H. J. ; Zhang, W. Q. ; Qiu, H. ; Zhang, G. ; Li, X. ; Qi, H. P. ; Guo, J. Z. ; Qian, J. ; Shi, X. L. ; Gao, X. ; Shi, D. K. ; Zhang, D. Y. ; Gao, R. L. ; Ding, J. D. A biodegradable metal-polymer composite stent safe and effective on physiological and serum-containing biomimetic conditions. *Adv. Healthc. Mater.* **2022**, *11*, 2201740.
8 Mehta, R.; Kumar, V.; Bhunia, H.; Upadhyay, S. N. Synthesis of poly (lactic acid): a review. *J. Macromol. Sci., Polym. Rev.* **2005**, *45*, 325–349.
9 Cui, S. Q.; Yu, L.; Ding, J. D. Thermogelling of amphiphilic block copolymers in water: ABA type versus AB or BAB type. *Macromolecules* **2019**, *52*, 3697–3715.
10 Albertsson, A. C.; Varma, I. K. Recent developments in ring opening polymerization of lactones for biomedical applications. *Biomacromolecules* **2003**, *4*, 1466–1486.
11 Dijkstra, P. J.; Du, H.; Feijen, J. Single site catalysts for stereoselective ring-opening polymerization of lactides. *Polym. Chem.* **2011**, *2*, 520–527.
12 Zhang, X.; Fevre, M.; Jones, G. O.; Waymouth, R. M. Catalysis as an enabling science for sustainable polymers. *Chem. Rev.* **2018**, *118*, 839–885.
13 Bartnikowski, M.; Dargaville, T. R.; Ivanovski, S.; Hutmacher, D. W. Degradation mechanisms of polycaprolactone in the context of chemistry, geometry and environment. *Prog. Polym. Sci.* **2019**, *96*, 1–20.
14 Chen, W. H.; Chen, Q. W.; Chen, Q.; Cui, C. Y; Duan, S.; Kang, Y. Y.; Liu, Y.; Muhammad, W.; Shao, S. Q.; Tang, C. Q.; Wang, J. Q.; Wang, L.; Xiong, M. H.; Yin, L. C.; Zhang, K.; Zhang, Z. Z.; Zhen, X.; Feng, J.; Gao, C. Y.; Gu, Z.; He, C. L.; Ji, J.; Jiang, X. Q.; Liu, W. G.; Liu, Z.; Peng, H. S.; Shen, Y. Q.; Shi, L. Q.; Sun, X. M.; Wang, H.; Wang, J.; Xiao, H. H.; Xu, F. J.; Zhong, Z. Y.; Zhang, X. Z.; Chen, X. S. Biomedical polymers: synthesis, properties, and applications. *Sci. China Chem.* **2022**, *65*, 1010–1075.

15 Wu, J. C.; Yu, T. L.; Chen, C. T.; Lin, C. C. Recent developments in main group metal complexes catalyzed/initiated polymerization of lactides and related cyclic esters. *Coord. Chem. Rev.* **2006**, *250*, 602–626.
16 Platel, R. H.; Hodgson, L. M.; Williams, C. K. Biocompatible initiators for lactide polymerization. *Polym. Rev.* **2008**, *48*, 11–63.
17 Dutta, S.; Hung, W. C.; Huang, B. H.; Lin, C. C. Recent developments in metal-catalyzed ring-opening polymerization of lactides and glycolides: preparation of polylactides, polyglycolide, and poly(lactide-*co*-glycolide). *Adv. Polym. Sci.* **2012**, *245*, 219–283.
18 Kowalski, A.; Libiszowski, J.; Biela, T.; Cypryk, M.; Duda, A.; Penczek, S. Kinetics and mechanism of cyclic esters polymerization initiated with tin(II) octoate. Polymerization of ε-caprolactone and L,L-lactide co-initiated with primary amines. *Macromolecules* **2005**, *38*, 8170–8176.
19 Bednarek, M. Branched aliphatic polyesters by ring-opening (co)polymerization. *Prog. Polym. Sci.* **2016**, *58*, 27–58.
20 Fuoco, T.; Pappalardo, D. Aluminum alkyl complexes bearing salicylaldiminato ligands: versatile initiators in the ring-opening polymerization of cyclic esters. *Catalysts* **2017**, *7*, 64.
21 Jiang, H. J.; He, J. P.; Liu, J. P.; Yang, Y. L. Synthesis and characterization of poly(ethylene-*co*-vinyl alcohol)-graft-poly(ε-caprolactone). *Polym. J.* **2002**, *34*, 682–686.
22 Xiang, S.; Zhou, D. D.; Feng, L. D.; Bian, X. C.; Li, G.; Chen, X. S.; Wang, T. C. Influence of chain architectures on crystallization behaviors of PLLA block in PEG/PLLA block copolymers. *Chinese J. Polym. Sci.* **2019**, *37*, 258–267.
23 Cui, S. Q.; Chen, L.; Yu, L.; Ding, J. D. Synergism among polydispersed amphiphilic block copolymers leading to spontaneous physical hydrogelation upon heating. *Macromolecules* **2020**, *53*, 7726–7739.
24 Cai, C. Y.; Tang, J. Y. Zhang, Y.; Rao, W. H.; Cao, D. L. G.; Guo, W.; Yu, L.; Ding, J. D. Intelligent paper-free sprayable skin mask based on an *in situ* formed Janus hydrogel of an environment-friendly polymer. *Adv. Healthc. Mater.* **2022**, *11*, 2102654.
25 Peng, Y. M.; Liu, Q. J.; He, T. L.; Ye, K.; Yao, X.; Ding, J. D. Degradation rate affords a dynamic cue to regulate stem cells beyond varied matrix stiffness. *Biomaterials* **2018**, *178*, 467–480.
26 Lecomte, P.; Riva, R.; Jérôme, C.; Jérôme, R. Macromolecular engineering of biodegradable polyesters by ring-opening polymerization and 'click' chemistry. *Macromol. Rapid Commun.* **2008**, *29*, 982–997.
27 Chen, T. T.; Cai, T. J.; Jin, Q.; Ji, J. Design and fabrication of functional polycaprolactone. *e-Polymers* **2015**, *15*, 3–13.
28 d'Arcy, R.; Burke, J.; Tirelli, N. Branched polyesters: preparative strategies and applications. *Adv. Drug Deliv. Rev.* **2016**, *107*, 60–81.
29 Xu, Y. C.; Ren, W. M.; Zhou, H.; Gu, G. G.; Lu, X. B. Functionalized polyesters with tunable degradability prepared by controlled ring-opening (co)polymerization of lactones. *Macromolecules* **2017**, *50*, 3131–3142.
30 Eyring, H. The activated complex in chemical reactions. *J. Chem. Phys.* **1935**, *3*, 107–115.
31 Evans, M. G.; Polanyi, M. Some applications of the transition state method to the calculation of reaction velocities, especially in solution. *Trans. Faraday Soc.* **1935**, *31*, 875–894.
32 Laidler, K. J.; King, M. C. The development of transition-state theory. *J. Phys. Chem.* **1983**, *87*, 2657–2664.
33 Polanyi, J. C. Some concepts in reaction dynamics. *Science* **1987**, *236*, 680–690.
34 Orio M.; Pantazis, D. A. Neese, F. Density functional theory. *Photosynth. Res.* **2009**, *102*, 443–453.
35 Shang, C.; Liu, Z. P. Constrained broyden dimer method with bias potential for exploring potential energy surface of multistep reaction process. *J. Chem. Theory Comput.* **2012**, *8*, 2215–2222.
36 Bo, X. X.; Zheng, H. F.; Xin, J. F.; Ding, Y. H. A kinetically persistent isomer found for pentazole: a global potential energy surface survey. *Chem. Commun.* **2019**, *55*, 2597–2600.
37 Wu, F. L; Huang, Y. D.; Yu, F. Z.; Li, Z. H.; Ding, C. F. Effect of transition-metal Ions on the conformation of encephalin investigated by hydrogen/deuterium exchange and theoretical calculations. *J. Phys. Chem. B* **2020**, *124*, 101–109.
38 Han, J. R.; Wu, F. L.; Yang, S. T.; Wu, X. N.; Tang, K. Q.; Li, Z. H.; Ding, C. F. Conformation changes of enkephalin in coordination with $Pb^{2+}$ Investigated by gas phase hydrogen/deuterium exchange mass spectrometry combined with theoretical calculations. *Chem. Res. Chin. Univ.* **2022**, *38*, 572–578.
39 Zhao, Y.; Truhlar, D. G. Density functionals with broad applicability in chemistry. *Acc. Chem. Res.* **2008**, *41*, 157–167.
40 Marlier, E. E.; Macaranas, J. A.; Marell, D. J.; Dunbar, C. R.; Johnson, M. A.; DePorre, Y.; Miranda, M. O.; Neisen, B. D.; Cramer, C. J.; Hillmyer, M. A.; Tolman, W. B. Mechanistic studies of ε-caprolactone polymerization by (salen) alor complexes and a predictive model for cyclic ester polymerizations. *ACS Catal.* **2016**, *6*, 1215–1224.
41 Nifant'ev, I. E.; Ivchenko, P. Coordination ring-opening polymerization of cyclic esters: A critical overview of DFT modeling and visualization of the reaction mechanisms. *Molecules* **2019**, *24*, 4117.
42 Allen, M. P.; Tildesley, D. J. *Computer simulation of liquids*. Oxford University Press, **2017**.
43 Binder, K. ; Heermann, D. W. *Monte Carlo simulation in statistical physics*. Springer-Verlag Berlin, **2010**.
44 Xu, G. Q.; Ding, J. D.; Yang, Y. L. Monte Carlo simulation of self-avoiding lattice chains subject to simple shear flow. I. Model and simulation algorithm. *J. Chem. Phys.* **1997**, *107*, 4070.
45 Luo, Z. L.; Ding, J. D.; Zhou, Y. Q. Temperature-dependent folding pathways of Pin1 WW domain: an all-atom molecular dynamics simulation of a Gō model. *Biophys. J.* **2007**, *93*, 2152–2161.
46 Cui, S.; Yu, Q. L.; Ding, J. D. Semi-bald micelles and corresponding percolated micelle networks of thermogels. *Macromolecules* **2018**, *51*, 6405–6420.
47 Cui, S. Q.; Yu, L.; Ding, J. D. Strategy of "block blends" to generate polymeric thermogels versus that of one-component block copolymer. *Macromolecules* **2020**, *53*, 11051–11064.
48 Gao, H. B.; Li, H.; Zhang, X. Q.; Wang, X. H.; Li, C. Y.; Luo, M. B. Computer simulation study on adsorption and conformation of polymer chains driven by external force. *Chinese J. Polym. Sci.* **2021**, *39*, 258–266.
49 Ma, R.; Xu, D.; Luo, C. F. Effect of crystallization and entropy contribution upon the mechanical response of polymer nano-fibers: a steered molecular dynamics study. *Chinese J. Polym. Sci.* **2023**, *41*, 465–474.
50 Jeong, B.; Bae, Y. H.; Lee, D. S.; Kim, S. W. Biodegradable block copolymers as injectable drug-delivery systems. *Nature* **1997**, *388*, 860–862.
51 Yu, L.; Ding, J. D. Injectable hydrogels as unique biomedical materials. *Chem. Soc. Rev.* **2008**, *37*, 1473–1481.
52 Tabthong, S.; Nanok, T.; Sumrit, P.; Kongsaeree, P.; Prabpai, S.; Chuawong, P.; Hormnirun, P. Bis(pyrrolidene) schiff base aluminum complexes as isoselective-biased initiators for the controlled ring-opening polymerization of rac-lactide: experimental and theoretical studies. *Macromolecules* **2015**, *48*, 6846–6861.
53 Hong, M.; Chen, E. Y. X. Completely recyclable biopolymers with linear and cyclic topologies *via* ring-opening polymerization of γ-butyrolactone. *Nat. Chem.* **2016**, *8*, 42–49.
54 Gesslbauer, S.; Savela, R.; Chen, Y.; White, A. J. P.; Romain, C. Exploiting noncovalent interactions for room-temperature heteroselective rac-lactide polymerization using aluminum catalysts. *ACS Catal.* **2019**, *9*, 7912–7920.
55 Rao, W. H.; Cai, C. Y.; Tang, J. Y.; Wei, Y. M.; Gao, C. Y.; Yu, L.; Ding, J. D. Coordination insertion mechanism of ring-opening polymerization of lactide catalyzed by stannous octoate. *Chin. J.*

*Chem.* **2021**, *39*, 1965–1974.
56 Zhao, Y.; Truhlar, D. G. The M06 suite of density functionals for main group thermochemistry, thermochemical kinetics, noncovalent interactions, excited states, and transition elements: two new functionals and systematic testing of four M06-class functionals and 12 other functionals. *Theor. Chem. Acc.* **2008**, *120*, 215–241.
57 Goerigk, L.; Grimme, S. A thorough benchmark of density functional methods for general main group thermochemistry, kinetics, and noncovalent interactions. *Phys. Chem. Chem. Phys.* **2011**, *13*, 6670–6688.
58 Grimme, S.; Antony, J.; Ehrlich, S.; Krieg, H. A consistent and accurate ab initio parametrization of density functional dispersion correction (DFT-D) for the 94 elements H-Pu. *J. Chem. Phys.* **2010**, *132*, 154104.
59 Weigend, F.; Ahlrichs, R. Balanced basis sets of split valence, triple zeta valence and quadruple zeta valence quality for H to Rn: design and assessment of accuracy. *Phys. Chem. Chem. Phys.* **2005**, *7*, 3297–3305.
60 Gaussian 09, Revision D. 01, Frisch, M. J.; Trucks, G. W.; Schlegel, H. B.; Scuseria, G. E.; Robb, M. A.; Cheeseman, J. R.; Scalmani, G.; Barone, V.; Mennucci, B.; Petersson, G. A.; Nakatsuji, H.; Caricato, M.; Li, X.; Hratchian, H. P.; Izmaylov, A. F.; Bloino, J.; Zheng, G.; Sonnenberg, J. L.; Hada, M; Ehara, M.; Toyota, K.; Fukuda, R.; Hasegawa, J.; Ishida, M.; Nakajima, T.; Honda, Y.; Kitao, O.; Nakai, H.; Vreven, T.; Montgometry, J. A.; Jr.; Peralta, J. E.; Ogliaro, F.; Bearpark, M.; Heyd, J. J.; Brothers, E.; Kudin, K. N.; Staroverov, V. N.; Kobayashi, R.; Normand, J.; Raghavachari, K.; Rendell, A.; Burant, J. C.; Iyengar, S. S.; Tomasi, J.; Cossi, M.; Rega, N.; Millam, J. M.; Klene, M.; Knox, J. E.; Cross, J. B.; Bakken, V.; Adamo, C.; Jaramillo, J.; Gomperts, R.; Stratmann, R. E.; Yazyev, O.; Austin, A. J.; Cammi, R.; Pomelli, C.; Ochterski, J. W.; Martin, R. L.; Morokuma, K.; Zakrzewski, V. G.; Voth, G. A.; Salvador, P.; Dannenberg, J. J.; Dapprich, S.; Daniels, A. D.; Farkas, Ö.; Foresman, J. B.; Ortiz, J. V.; Cioslowski, J.; Fox, D. J. Gaussian, Inc. Wallingford CT, **2016**.
61 Tian Lu, Molclus program, Version 1.9. 9.9, http://www.keinsci.com/research/molclus.html
62 Lawan, N.; Muangpil, S.; Kungwan, N.; Meepowpan, P.; Lee, V. S.; Punyodom, W. Tin (IV) alkoxide initiator design for poly(d-lactide) synthesis using DFT calculations. *Comput. Theor. Chem.* **2013**, *1020*, 121–126.
63 Della Monica, F.; Luciano, E.; Roviello, G.; Grassi, A.; Milione, S.; Capacchione, C. Group 4 metal complexes bearing thioetherphenolate ligands. coordination chemistry and ring-opening polymerization catalysis. *Macromolecules* **2014**, *47*, 2830–2841.
64 Chang, M. C.; Lu, W. Y.; Chang, H. Y.; Lai, Y. C.; Chiang, M. Y.; Chen, H. Y.; Chen, H. Y. Comparative study of aluminum complexes bearing N,O- and N,S-Schiff base in ring-opening polymerization of ε-caprolactone and L-lactide. *Inorg. Chem.* **2015**, *54*, 11292–11298.
65 Ligny, R.; Hänninen, M. M.; Guillaume, S. M.; Carpentier, J. F. Highly syndiotactic or isotactic polyhydroxyalkanoates by ligand-controlled yttrium-catalyzed stereoselective ring-opening polymerization of functional racemic β-lactones. *Angew. Chem. Int. Ed.* **2017**, *129*, 10524–10529.
66 Nifant'ev, I. E.; Shlyakhtin, A. V.; Bagrov, V. V.; Minyaev, M. E.; Churakov, A. V.; Karchevsky, S. G.; Birin, K. P.; Ivchenko, P. V. Mono-BHT heteroleptic magnesium complexes: synthesis, molecular structure and catalytic behavior in the ring-opening polymerization of cyclic esters. *Dalton Trans.* **2017**, *46*, 12132–12146.
67 Jitonnom, J.; Molloy, R.; Punyodom, W.; Meelua, W. Theoretical studies on aluminum trialkoxide-initiated lactone ring-opening polymerizations: roles of alkoxide substituent and monomer ring structure. *Comput. Theor. Chem.* **2016**, *1097*, 25–32.
68 Stevels, W. M.; Ankoné, M. J.; Dijkstra, P. J.; Feijen, J. Kinetics and mechanism of ε-caprolactone polymerization using yttrium alkoxides as initiators. *Macromolecules* **1996**, *29*, 8296–8303.
69 O'Keefe, B. J.; Hillmyer, M. A.; Tolman, W. B. Polymerization of lactide and related cyclic esters by discrete metal complexes. *J. Chem. Soc., Dalton Trans.* **2001**, *15*, 2215–2224.
70 Chen, E. Y. X. Coordination polymerization of polar vinyl monomers by single-site metal catalysts. *Chem. Rev.* **2009**, *109*, 5157–5214.
71 Penczek, S.; Cypryk, M.; Duda, A.; Kubisa, P.; Slomkowski, S. Living ring-opening polymerizations of heterocyclic monomers. *Prog. Polym. Sci.* **2007**, *32*, 247–282.
72 Neffgen, S.; Keul, H.; Höcker, H. Ring-opening polymerization of cyclic urethanes and ring-closing depolymerization of the respective polyurethanes. *Macromol. Rapid Commun.* **1996**, *17*, 373–382.
73 Wu, D. C.; Xu, F. Sun, B. Fu, R. W.; He, H. K.; Matyjaszewski, K. Design and preparation of porous polymers. *Chem. Rev.* **2012**, *112*, 3959–4015.
74 Baumgartner, R. Fu, H. L.; Song, Z. Y.; Lin, Y.; Cheng, J. J. Cooperative polymerization of α-helices induced by macromolecular architecture. *Nat. Chem.* **2017**, *9*, 614–622.
75 Xia, Y. C.; Song, Z. Y.; Tan, Z. Z.; Xue, T. R.; Wei, S. Q.; Zhu, L. Y.; Yang, Y. F.; Fu, H. L.; Jiang, Y. J.; Lin, Y.; Ferguson, A. L.; Cheng, J. J. Accelerated polymerization of *N*-carboxyanhydrides catalyzed by crown ether. *Nat. Commun.* **2021**, *12*, 732.
76 Yu, X. Y.; Li, G. H.; Zheng, Y. K.; Gao, J. M.; Fu, Y.; Wang, Q. S.; Pan, X. G.; Huang, L.; Ding, J. D. "Invisible" orthodontics by polymeric "clear" aligners molded by 3D-printed personalized dental models. *Regen. Biomater.* **2022**, *9*, rbac007.
77 Gao, J. M.; Ding, X. Q.; Yu, X. Y.; Chen, X. B.; Zhang, X. Y.; Cui, S. Q.; Shi, J. Y.; Chen, J.; Yu, L.; Chen, S. Y.; Ding, J. D. Cell-free bilayered porous scaffolds for osteochondral regeneration fabricated by continuous 3D-printing using nascent physical hydrogel as ink. *Adv. Healthc. Mater.* **2021**, *10*, 1–13.
78 Wang, F. S.; Zhao, X. J.; Cao, Y.; Qian, R. Y. A comparison of polyacetylenes prepared with various catalyst systems. *Chinese J. Polym. Sci.* **1985**, *2*, 180–184.
79 Engle, K. M.; Mei, T. S.; Wasa, M.; Yu, J. Q. Weak coordination as a powerful means for developing broadly useful C–H functionalization reactions. *Acc. Chem. Res.* **2012**, *45*, 788–802.
80 Romero, N. A.; Nicewicz, D. A. Organic photoredox catalysis. *Chem. Rev.* **2016**, *116*, 10075–10166.
81 Liu, L. C.; Corma, A. Metal catalysts for heterogeneous catalysis: from single atoms to nanoclusters and nanoparticles. *Chem. Rev.* **2018**, *118*, 4981–5079.
82 Cao, D. L. G.; Guo, W.; Cai, C. Y.; Tang, J. Y.; Rao, W. H.; Wang, Y.; Wang, Y. B.; Yu, L.; Ding, J. D. Unified therapeutic-prophylactic vaccine demonstrated with a postoperative filler gel to prevent tumor recurrence and metastasis. *Adv. Funct. Mater.* **2022**, *32*, 2206084.
83 Kulkarni, A.; Siahrostami, S.; Patel, A.; Nørskov, J. K. Understanding catalytic activity trends in the oxygen reduction reaction. *Chem. Rev.* **2018**, *118*, 2302–2312.
84 Yu, H. Y.; Wang, J.; Shao, J. W.; Chen, D.; Wang, S. C.; Wang, L.; Yang, W. T. Controlled radical polymerization of styrene mediated by xanthene-9-thione and its derivatives. *Chinese J. Polym. Sci.* **2018**, *36*, 1303–1311.
85 Yu, Y.; Wang, X. L.; Zhu, Y.; He, Y. N.; Xue, H. R.; Ding, J. D. Is polydopamine beneficial for cells on the modified surface. *Regen. Biomater.* **2022**, *9*, rbac078.
86 Lu, X. B.; Ren, B. H. Partners in epoxide copolymerization catalysis: approach to high activity and selectivity. *Chinese J. Polym. Sci.* **2022**, *40*, 1331–1348.
87 Hammer, B.; Norskov, J. K. Why gold is the noblest of all the metals. *Nature* **1995**, *376*, 238–240.
88 Michaelides, A.; Liu, Z. P.; Zhang, C. J.; Alavi, A.; King, D. A.; Hu, P. Identification of general linear relationships between activation energies and enthalpy changes for dissociation reactions at

surfaces. *J. Am. Chem. Soc.* **2003**, *125*, 3704–3705.
89 Calle-Vallejo, F.; Loffreda, D.; Koper, M. T. M.; Sautet, P. Introducing structural sensitivity into adsorption-energy scaling relations by means of coordination numbers. *Nat. Chem.* **2015**, *7*, 403–410.
90 Tran, K.; Ulissi, Z. W. Active learning across intermetallics to guide discovery of electrocatalysts for $CO_2$ reduction and $H_2$ evolution. *Nat. Catal.* **2018**, *1*, 696–703.
91 Lopato, E. M.; Eikey, E. A.; Simon, Z. C. Back, S.; Tran, K.; Lewis, J.; Kowalewski, J. F.; Yazdi, S.; Kitchin, J. R.; Ulissi, Z. W.; Millstone, J. E.; Bernhard, S. Parallelized screening of characterized and DFT-modeled bimetallic colloidal cocatalysts for photocatalytic hydrogen evolution. *ACS Catal.* **2020**, *10*, 4244–4252.
92 Shen, T. H.; Yang, Y. Q.; Xu, X. Structure-reactivity relationship for nano-catalysts in the hydrogenation/dehydrogenation controlled reaction systems. *Angew. Chem. Int. Ed.* **2021**, *133*, 26546–26549.
93 Essa, D.; Kondiah, P. P.; Choonara, Y. E.; Pillay, V. The design of poly(lactide-*co*-glycolide) nanocarriers for medical applications. *Front. Bioeng. Biotech.* **2020**, *8*, 48.
94 Xu, X.; Gao, J. m.; Liu, S. Y.; Chen, L. Chen, M.; Yu, X. Y.; Ma, N.; Zhang, J.; Chen, X. B.; Zhong, L. S.; Yu, L.; Xu, L. M.; Guo, Q. Y.; Ding, J. D. Magnetic resonance imaging for non-invasive clinical evaluation of normal and regenerated cartilage. *Regen. Biomater.* **2021**, *8*, rbab038.
95 Wang, G.; Gao, C. Y.; Xiao, B. H.; Zhang, J. Jiang, X. Y.; Wang, Q. S.; Guo, J. Z.; Zhang, D. Y.; Liu, J. X.; Xie, Y. H.; Shu, C. Ding, J. D. Research and clinical translation of trilayer stent-graft of expanded polytetrafluoroethylene for interventional treatment of aortic dissection. *Regen. Biomater.* **2022**, *9*, rbac049.
96 Wang, R. Z.; Huang, S.; Zhang, Q. Y.; Yu, X. S.; Hong, K. Z.; Cao, J. R.; Xiao, H.; Wang, Y.; Shuai, X. T. Construction of magnetic resonance imaging visible polymeric vector for efficient tumor targeted siRNA delivery. *Chinese J. Polym. Sci.* **2022**, *40*, 1071–1079.
97 Gao, C. Y.; Wang, G.; Wang, L.; Wang, Q. S.; Wang, H. C.; Yu, L.; Liu, J. X.; Ding, J. D. A biosurfactant-containing TSD strategy to modify bovine pericardial bioprosthetic valves for anticalcification. *Chinese J. Polym. Sci.* **2023**, *41*, 51–66.
98 Cao, D. L. G.; Ding, J. D. Recent advances in regenerative biomaterials. *Regen. Biomater.* **2022**, *9*, rbac098.

https://doi.org/10.1007/s10118-023-2930-6